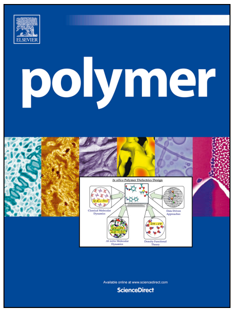

Synthesis and evaluation of new radical photoinitiators bearing trialkoxysilyl groups for surface immobilization

Piotr Roszkowski, Melahat Sahin, Santhosh Ayalur-Karunakaran, Christoph Gammer, Sandra Schlögl, Wolfgang Kern, Krzysztof K. Krawczyk

PII: S0032-3861(17)30927-8
DOI: 10.1016/j.polymer.2017.09.054
Reference: JPOL 20023

To appear in: *Polymer*

Received Date: 11 July 2017
Revised Date: 15 September 2017
Accepted Date: 23 September 2017

Please cite this article as: Roszkowski P, Sahin M, Ayalur-Karunakaran S, Gammer C, Schlögl S, Kern W, Krawczyk KK, Synthesis and evaluation of new radical photoinitiators bearing trialkoxysilyl groups for surface immobilization, *Polymer* (2017), doi: 10.1016/j.polymer.2017.09.054.

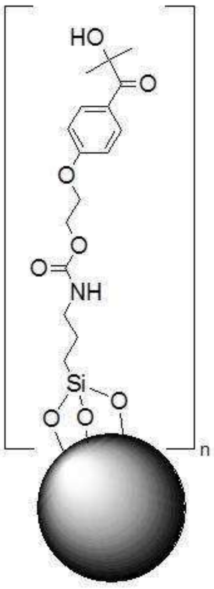
HO
O
O
O
O
NH
Si
O
O
O
n

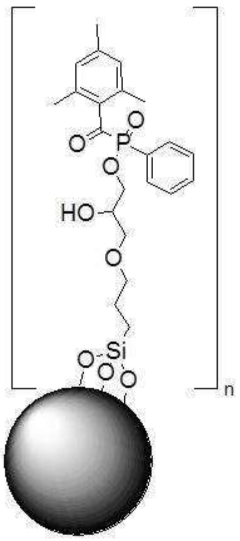
O
P
O
O
HO
O
Si
O
O
O
n

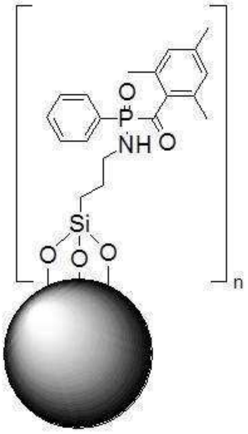
O
P
NH
O
Si
O
O
O
n

Synthesis and evaluation of new radical photoinitiators bearing trialkoxysilyl groups for surface immobilization

Piotr Roszkowski,[1,2] Melahat Sahin,[3] Santhosh Ayalur-Karunakaran,[3] Christoph Gammer,[4] Sandra Schlögl,[3] Wolfgang Kern,[1,3] Krzysztof K. Krawczyk[1,]*

Affiliations:

1. *Chair in Chemistry of Polymeric Materials, Montanuniversitaet Leoben, Otto Glöckel-Straße 2, 8700 Leoben, Austria*
2. *Faculty of Chemistry, University of Warsaw, Pasteura 1, 02-093 Warsaw, Poland*
3. *Polymer Competence Center Leoben GmbH, Roseggerstraße 12, 8700 Leoben, Austria*
4. *Erich Schmid Institute of Materials Science, Austrian Academy of Sciences, Jahnstrasse 12, 8700 Leoben, Austria.*

E-mail: *k.k.krawczyk@unileoben.ac.at*

ABSTRACT

Photoinitiators, which can be readily immobilized on surfaces, *e.g.* on the surface of nanoparticles, have gained considerable attention of both scientists and engineers. The main reason for this interest is that immobilized initiators lead to a covalent linkage between the surface and the resulting polymer chain. Thus, immobilized photoinitiators are expected not to migrate out of the polymer network, which reduces potential health risks. This paper describes the synthesis of a range of short- and long-wavelength absorbing photoinitiators bearing trialkoxysilyl units. The synthesis starts from commercially available products, Irgacure 2959 or Irgacure TPO-L, and takes 1-4 steps. While some of the reported initiators were previously sparsely described in patents, but lack a systematic study, others are reported for the first time. Both free and immobilized initiators were characterized and tested with regard to their efficiency in acrylic and thiol-ene systems. The findings confirm the good applicability of the nanoparticle-immobilized photoinitiators in the preparation of nanocomposite materials.

Keywords: Photoinitiators, Irgacure TPO-L, Irgacure 2959, silanization, surface functionalization, nanocomposites

I. Introduction

Photoinitiators can trigger polymerization on demand, with high spatial and temporal resolution [1,2]. Thus, they have found broad application in technological processes such as the curing of adhesives[3], inks[4], coatings[5] as well as in photolithography and 3D printing.[6–8] The thermal stability of photoinitiators allows them to be stored in a polymerizable medium for long time, without any unwanted background reaction. Upon irradiation, the polymerization occurs quickly, whereas the amount of generated radicals can be tuned with the dose of irradiation. Moreover, some photoinitiators show a practical two-photon absorption phenomenon,[8,9] which is used in two-photon lithography.[10]

In Norrish type I photoinitiators the absorption of light leads to the formation of at least two radicals, [11] which can initiate the polymerization of an appropriate mixture of monomers. Two scenarios are possible: (a) the radical fragment, which initiates the polymerization, gets incorporated into the polymer, or (b) it recombines to form non-polymerizing residual molecules. The first scenario implies that after complete polymerization a part of the photoinitiator molecule is covalently attached to the polymer. If the initiator is bound to a surface it will thus serve as a linker between the surface and the polymer matrix. This phenomenon can be used in the preparation of composite materials [12,13] and the modification of functional surfaces with polymer brushes.[14] As a result of the second scenario, the recombined fragments of the initiator are not covalently attached to the polymer, and can migrate out of the material, causing malodor and potential health risks. A particular advantage of nanoparticle-bound photoinitiators is that the residual initiator molecules are attached to the particles. This is expected to greatly decrease their ability to migrate, and will thus reduce potential risks, *e.g.*, in biomedical applications or food packaging.[15]

The concept of surface initiated polymerization has been reviewed in the literature [16], with emphasis on so called ‘living’ radical polymerization,[17,18] also including the initiation from nanoparticle surfaces.[19–21] The covalent linkage of Norrish type I initiators to surfaces has been studied to a lesser extent in research papers, [12,13,22–25] although the amount of patents dealing with the subject suggests that it is an area of significant industrial interest [26–29].

Surface silanization is known to be one of the most efficient and practical ways to link organic functional molecules to surfaces, *e.g.* nanoparticle surfaces, and has been already applied in our laboratory [23,30]. The modification of nanoparticles can be achieved by, first, functionalizing their surface with reactive groups, and then coupling the desired functionality using a chemical reaction at the interface (linear strategy) [30], or by directly using a functional alkoxysilane [24,31] for silanization (convergent strategy). We chose the latter strategy, since it reduces the amount of diffusion limited reactions at the interface, and yields a product free of any undesired impurities.

Some of the silane-photoinitiators described in this paper were previously reported in patents [26–28] but the details of synthesis, characterization and evaluation are sparsely described or even missing, thus limiting their practical potential in research. The aim of this paper is to describe the details of the synthesis of selected photoinitiators for surface silanization, and evaluate their photochemical properties before and after deposition on the surface of a commercial silica nanopowder. As model photoinitiators, and the starting product of our preparations, we use the short wavelength absorbing initiator 2-hydroxy-4'-(2-hydroxyethoxy)-2-methylpropiophenone (Irgacure 2959, **1**) and the long wavelength absorbing ethyl (2,4,6-trimethylbenzoyl) phenylphosphinate (Irgacure TPO-L, **2**), which also exhibits 2-photon absorption properties [32].

II. Results and discussion

Synthesis of photocleavable silanes

The trialkoxysilyl terminated photoinitiators were synthesized from the commercially available photoinitiators in 1-4 steps, as presented in Scheme 1. The short wavelength absorbing photoinitiator **3** was synthesized by direct coupling of compound **1** to 3-(triethoxysilyl)propyl isocyanate. Although this reaction does not proceed in the absence of a catalyst [28] (as suggested by some literature [26,27]) the addition of a base, such as triethylamine, allowed almost complete conversion of the substrate to the corresponding urethane. Best results were obtained when the amine was used at a concentration of at least 10 mol%. The catalytic reaction is slow and takes approx. 120 h to complete at room temperature. At 70 ˚C the reaction was completed overnight, and the purified product was obtained in good yield.

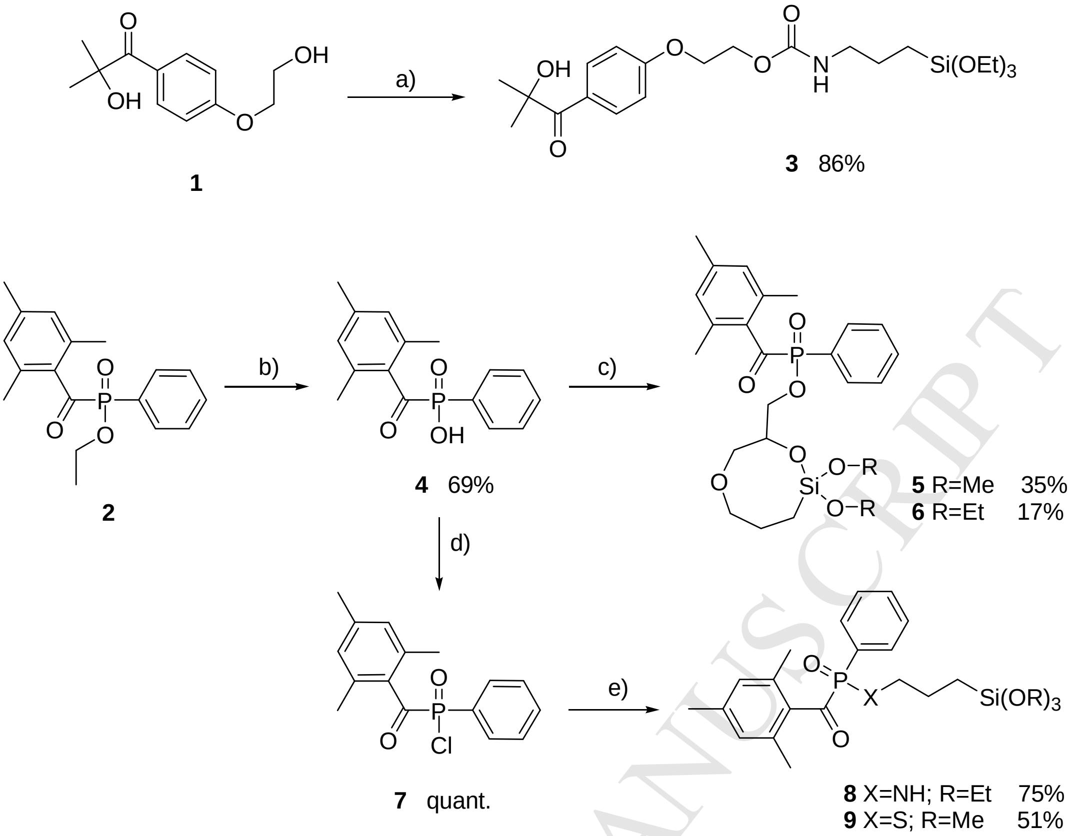

Scheme 1. Synthesis of the trialkoxysilane derivatives from commercially available photoinitiators; a) 3-(triethoxysilyl)propyl isocyanate, Et_3N, 2-butanone; b) 1.NaI, DCM; 2. H_2SO_4; c) (3-glycidoxypropyl)trialkoxysilane, toluene; d) $(COCl)_2$, DCM; e) APTES or MPTMS/Et_3N, toluene.

In order to obtain the long wavelength absorbing photoinitiators, the starting compound **2** was first hydrolysed in the presence of sodium iodide, and acidified to obtain the free acid **4**, as described in the literature [29,33,34]. The phosphinic acid **4** is able to open the epoxide of (3-glycidoxypropyl)trialkoxysilane to yield the linear product **5-L** (Scheme 2). However, upon longer reaction times **5-L** was converted almost quantitatively to the cyclic compound **5**. A similar cyclization was previously observed for several silanes obtained from epoxy resins [35–41]. Interestingly, only product **5-L** is reported in the literature. Although we have isolated a sample of this compound and measured its ^{1}H-NMR spectrum, it contained a small amount of an unidentified impurity. Any attempt to increase the purity by column chromatography led to complete decomposition of the product. Also, the product was not stable enough to record a ^{13}C NMR, as it quickly converted to product **5**. The latter is obtained as a mixture of diastereomers, since the opening of the epoxide generates a second stereogenic centre. The presence of two diastereomers in approx. 1:1 molar ratio was confirmed by ^{1}H-NMR: two sets of similar signals were observed for the alkyl part of the molecule.

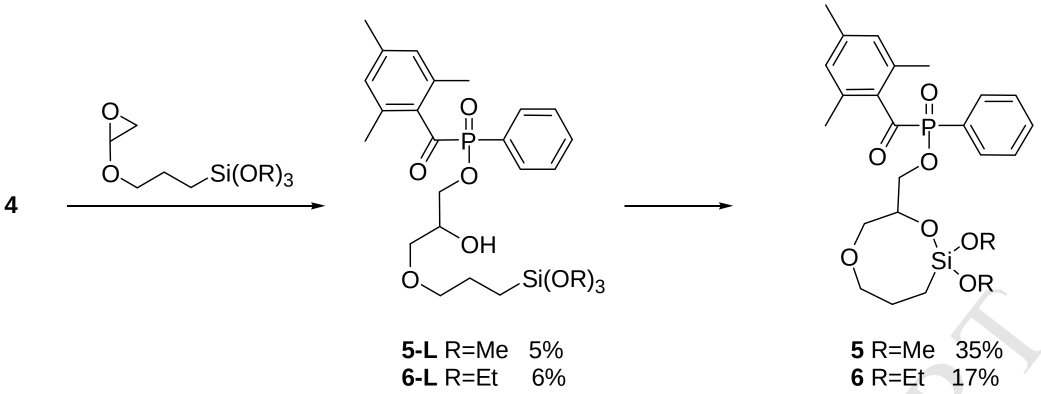

Scheme 2. Synthesis of the silane-functionalized photoinitiators from acid **4**. The alcohols **5-L** and **6-L** are spontaneously converted into their heterocyclic derivatives **5** and **6**.

In order to study the influence of the alkoxy group on the formation of the cyclic product, the 3-glycidoxypropyl)trimethoxysilane was replaced with its triethoxy derivative. Although also in this case the acyclic product was immediately accompanied by the cyclic derivative, the TLC screening of the reaction progress indicated that the cyclization occurs slower than in the case of the trimethoxy derivative. However, the linear derivative **6-L** also completely decomposed during a purification attempt.

Interestingly, in both compounds **5** and **6** the mesitylene ring shows a hindered rotation at room temperature, which results in the observation of two sets of signals from the *ortho*-methyl groups in ^{1}H-NMR.

Regarding the limited isolated yield of products **5** and **6**, a novel synthetic strategy was proposed to obtain trialkoxysilyl-derivatives of initiator **2**. First, acid **4** was converted to the corresponding acid chloride **7**. Although many variants of this transformation are described in the literature, [34,42–47] we have decided to modify the existing procedures and use oxalyl chloride to facilitate the workup. As expected, the resulting phosphinic acid chloride **7** reacted almost instantaneously with APTES to form the photoinitiator-silane **8**. This reaction proceeded best in the presence of 1 eq. of base to bind the chloride ion. An excess of APTES could also be used for this purpose. Surprisingly, we have found that upon longer reaction times, or during the evaporation of the solvent after the reaction, the base lead to partial decomposition of product **8**, accompanied by the appearance of a side product in the reaction mixture. The product was isolated and characterized as structure **10** (Scheme 3, left side). This undesired reactivity of product **8** was reduced by using a smaller excess of base, and by controlling the reaction time. It was also important to remove any excess of base after the reaction by washing with a dilute acid solution, before the solvent was evaporated. As a result, product **8** was isolated in pure form with a yield of 75% over two steps (starting from acid **4**). Interestingly, product **10** was also obtained in an attempt to synthesize amide **8** directly from the ester **2** (Scheme 3, right side).

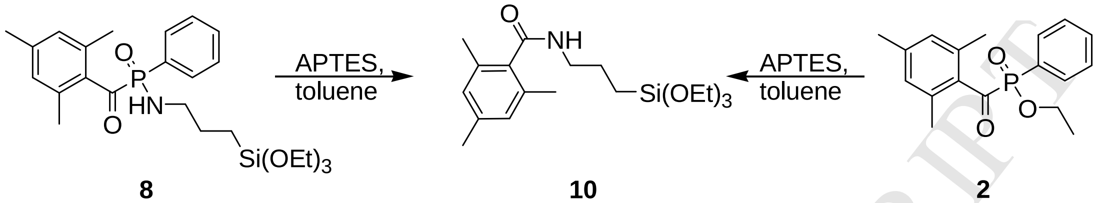

Scheme 3. Undesirded secondary reaction of compound **8** with the excess of APTES. Amide **10** is also obtained by direct reaction of APTES and photoinitiator **2**.

When the acid chloride **7** was treated with (3-mercaptopropyl)trimethoxysilane (MPTMS) in the presence of a base, product **9** was obtained. Although no decomposition products were observed, only an intermediate yield was achieved (51%).

Characterization of the reactivity of the photoinitiators

The obtained photoinitiator-silanes, as well as their parent photoinitiators, were characterized by photo-DSC in pure tetrahydrofurfuryl acrylate (THFA). In all cases, the concentration of the photoinitiator was adjusted to have the same molarity as the parent photoinitiator at 1% or 5% (w/w). The time to reach the maximum polymerization enthalpy, the maximum heat flow, and the full polymerization heat were determined and are summarized in Table 1.

Table 1. Summary of photo-DSC results. Values given in bold correspond to the 1 wt.% initiator content, and values given in standard font correspond to the 5 wt.% initiator content.

Sample name	$t_{\max}$ (s)		$H_{\max}$ (mW/mg)		ΔH (J/g)	
3	**7.05**	5.34	**-34.4**	-34.7	**-373.6**	-330.0
1	**7.47**	5.94	**-32.2**	-33.0	**-359.0**	-327.5
5	**3.90**	3.75	**-41.8**	-31.2	**-318.1**	-245.2
6	**3.81**	3.48	**-39.9**	-36.7	**-295.0**	-276.1
8	**4.05**	3.69	**-35.0**	-31.2	**-282.5**	-252.8
9	**4.89**	4.44	**-27.4**	-23.3	**-257.7**	-238.7

2	**3.99**	3.42	**-34.5**	-38.8	**-260.9**	-269.4

Initiator **3** was proven to be very photoreactive and even outperformed its parent photoinitiator **1**. The initiators **5** and **6**, which differ only in the size of the alkoxy groups, both showed a very similar reactivity, as expected, and also outperformed their parent initiator **2**. The APTES derived initiator **8** performed better than the MPTMS derived initiator **9**, and exhibited a photoreactivity very similar to photoinitiator **2**. Based on these results, and the yield in which the products were obtained, photoinitiators **3**, **5** and **8** were chosen for further studies and the immobilization on the surface of silica nanopowders.

The selected initiators were characterized by UV-Vis spectroscopy, and the results are summarized in Table 2. The molar absorption coefficients were determined for the two typical emission maxima from the Hg spectrum (254 and 365 nm), for the band at 390 nm, which is excitable *via* 2 photon absorption using a NIR laser operating at 780 nm [8], and for the wavelengths at which the initiators had their local absorption maxima (273 and 369 nm). The full UV-Vis spectra are presented in Fig. S1 in the Supporting Information.

Table 2. Molar absorption coefficients of the nanoparticle initiators. All values are reported in L·mol^{-1}·cm^{-1}.

Sample Name	ε at 254 nm	ε at 365 nm	ε at 390 nm	ε at 273nm (λmax$_1$)	ε at 369nm (λmax$_2$)
3	7804	-	-	18578	-
5	2679	236	175	2307	243
8	3127	259	229	2418	280

Immobilization of the photosensitive organosilanes on silica nanopowder

As the model nanopowder for the deposition of photoinitiators we have chosen the silica nanopowder (175-225 m^2/g, BET) from Sigma-Aldrich, which is a fumed silica consisting of intergrown nanograins, with typical size of 20-60 nm, forming larger clusters (agglomerates) with a broad size distribution ranging from approx. 100 nm to several µm in diameter (see the TEM images in Fig. 1).

The silanol content of the pristine silica was low, indicated by the barely noticeable broad absorption band around $\nu = 3400\ \text{cm}^{-1}$ in the IR spectrum [48] (Fig. 3).

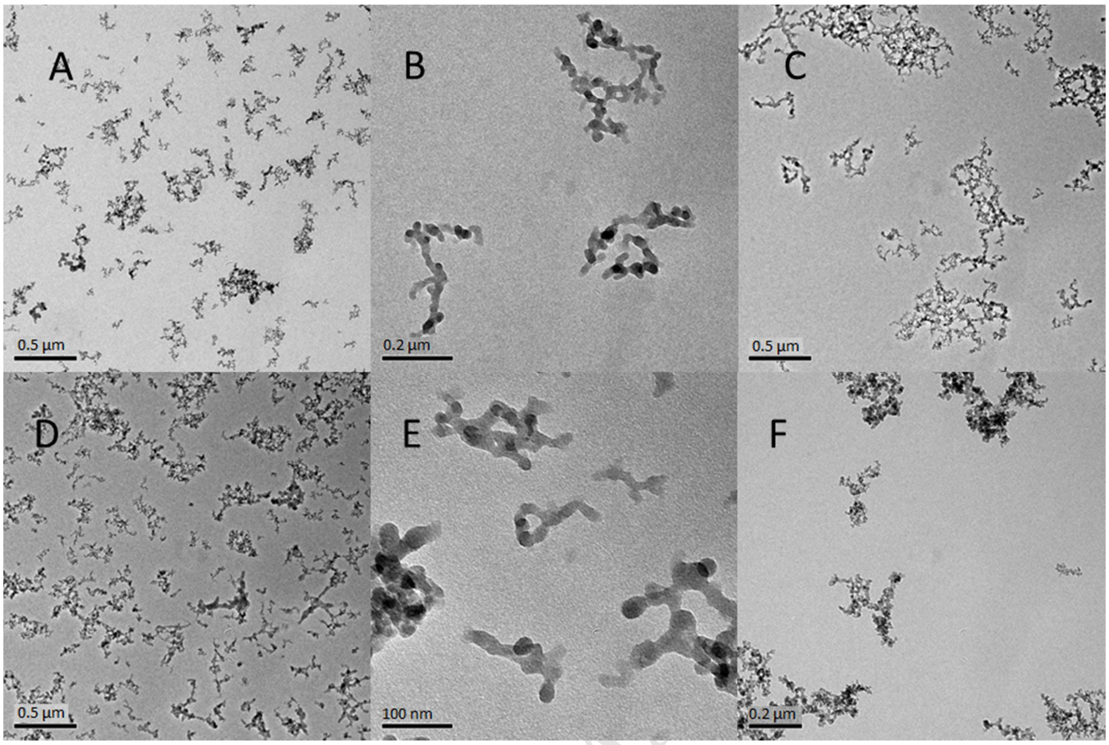

Figure 1. Typical TEM images of the pristine (A-C), and modified (D-F) silica nanopowder at different magnification. Images C and F show particles that have been purified by centrifugation. Please note the different scale bars.

The silica nanopowder was functionalized by silanization (Scheme 3). It was found that the functionalization of the pristine particles by simple incubation with the silane was inefficient, and most of the silane was recovered by washing. Thus, a different modification method was employed, which was already proven successful in our laboratory [23]. In this method (general method 1), the silanol content of the silica was increased by corona treatment. After silanization and washing, the modified particles **NPWD-3-M** (from silane **3**) showed an organic content of 2.55%, which corresponds to the immobilization of approx. 70 mol% of the used silane. This silanization method includes a washing step, which is not desirable for industrial applications, and leads to the removal of the fraction of small silica nanoparticles which cannot be collected by centrifugation. For that reason another silanization method was developed (general method 2) which is similar to the process of wet impregnation [49]. In this method the pristine silica nanopowder is reacted with the silane, first, under anhydrous conditions and in the presence of an acidic catalyst. In the second step a water containing solvent is added to complete the hydrolysis of the silane. To assure complete condensation of the hydrolysed silanes on the surface of the nanoparticles, the solvent is removed by evaporation, and the hydrolysis and evaporation process is repeated twice more. In this way the time consuming corona treatment and centrifugal washing of the nanopowder can be avoided. Using this method, the silica nanopowder was modified with silanes **3**, **5** and **8** yielding nanopowders **NPWD-3**, **NPWD-5** and **NPWD-8**, respectively (Scheme 4). It should be noted, that although the cyclic silyl ether **5** was used for the silanization, it was expected to hydrolyse under the applied conditions. As a result, mostly the linear form, as represented by structure **5-L,** is expected to be immobilized onto the silica nanopowder.

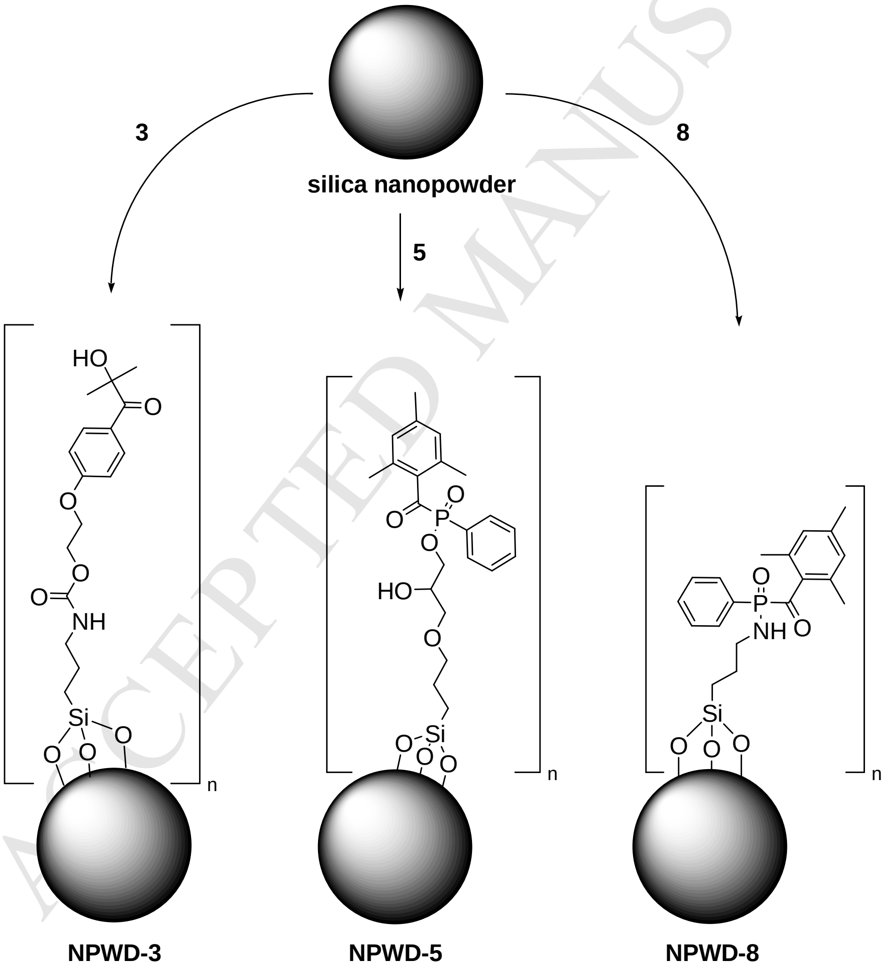

Scheme 4. Preparation of the silica-nanopowder grafted photoinitiators from the corresponding silane-functionalized initiators. Note, that although initiator **5** is used for the functionalization of the silica, it is expected to be immobilized mostly in its linear form (as represented by structure **5-L**).

The thermogravimetric analysis (TGA) confirmed a high organic content of the prepared silica nanopowders (Fig. 2, Table 3). After washing, the organic content of the powders decreased by 20-37%, which can be attributed to the removal of some unattached oligomeric condensates, but also to the loss of the fraction of small particles during washing. Such loss was expected, since we have observed that the mass of the nanopowder sample decreased significantly after every washing step (14.45% sample weight loss after the first washing step for **NPWD-3**; see footnote to Table 3). To prove that the supernatant from the washing did not contain significant amounts of non-attached polymer (*i.e.* soluble polycondensates of compound **3**) a TGA curve was recorded for the dried supernatant from **NPWD-3**. A weight loss of only 12.4% was observed, proving that this fraction still contained silica nanoparticles, albeit highly functionalized. From the TEM images in Fig. 1 it can be observed that the fraction of smallest nanoparticle agglomerates is being lost during the process of centrifugal washing. Assuming that the particles removed during centrifugation had an organic content of at least 7.11%, it can be calculated that over 90% of the hydrolysed silane **3** was covalently attached to the nanoparticles and precipitated during centrifugation (details of the calculations are described in the Supporting Information). This estimation is conservative, since it can be assumed that the fraction of smallest nanoparticles, which do not precipitate upon centrifugation, has the highest specific surface area and thus higher degree of functionalization (organic content) than the precipitate. To further confirm that this fraction contained only traces of physically attached oligomers, MALDI-MS studies were performed. For this purpose the dried supernatant from the washed particles was dispersed in a minimal amount of solvent, and subjected to filtration on a 0.2 μm filter, to eliminate most of the remaining silica. MALDI-MS of dried filtrates showed only trace amounts of ionisable material (MALDI MS spectra are shown in the Supporting Information).

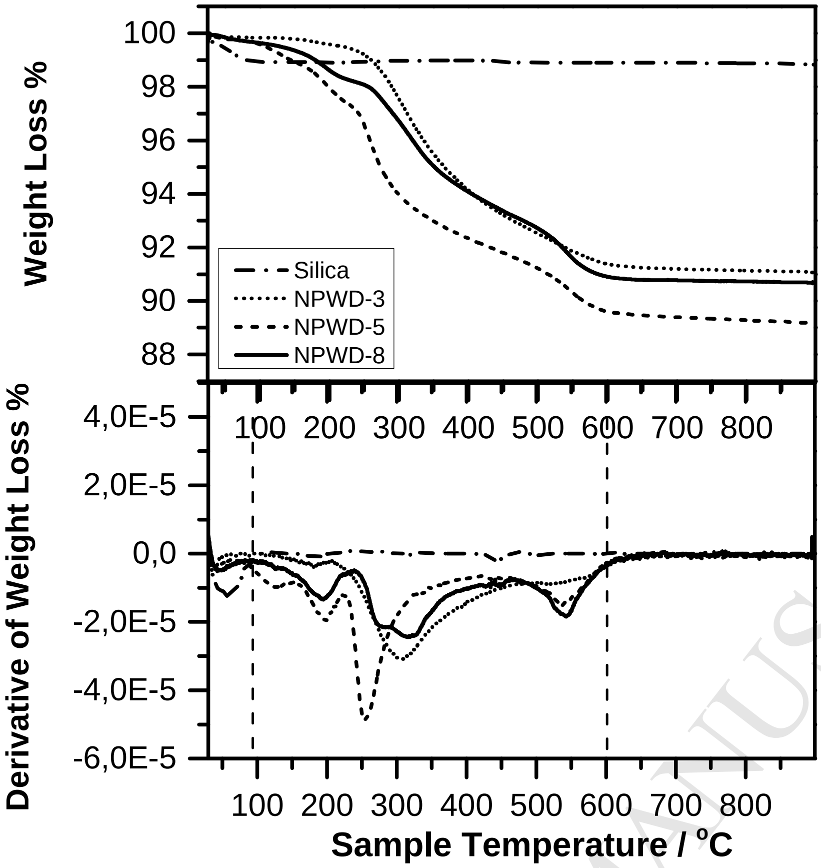

Figure 2. TGA curves of the pristine silica nanopowder and the prepared nanopowder-grafted photoinitiators.

Table 3. Overview of the TGA analysis of the reference sample (silica) and functionalized silica nanopowders.

Sample	TGA weight loss (% w/w)	TGA weight loss after washing (% w/w)
Silica	0.85	-
NPWD-3	8.92	7.11[*]
NPWD-5	10.6	6.73
NPWD-8	9.24	6.03
NPWD-3-M	-	2.55

*- The sample loss after the first washing was determined for **NPWD-3** by evaporation of the supernatant and was found to be 14.45% (w/w) of the pristine sample. The solid material obtained, showed a TGA weight loss of 12.40% (w/w).

The elemental composition of the silica-grafted photoinitiators was studied by combustion analysis (C,H,N) and classical analysis (P), and the results are summarized in Table 4.

Table 4. Elemental composition of the pristine silica and the unwashed, nanopowder-grafted photoinitiators.

Sample Name	**C (% w/w)**	**H (% w/w)**	**N (% w/w)**	**P (% w/w)**
Silica	0.85	0.20	<0.03	<0.05
NPWD-3	5.26	0.75	0.40	<0.05
NPWD-5	6.89	0.86	<0.03	0.69
NPWD-8	6.36	0.83	0.36	0.68

The molar absorption coefficients of the nanoparticle grafted initiators were determined at the same wavelengths as for the free trialkoxysilane derivatives. The absorption values from the direct measurement were significantly influenced by the scattering of UV-light on the silica nanopowder. Due to the scattering of the particles, the baseline of the curve shows a positive linear variation. To eliminate the scattering effect, a linear fit was estimated (see S3 in the Supporting Information) and then the absorbance values were determined. The values reported in Table 5 are corrected for the scattering.

Table 5. Molar absorption coefficients of the nanopowder-grafted initiators. All values are reported in L·mol^{-1}·cm^{-1}.

Sample name	ε at 254 nm	ε at 365 nm	ε at 390 nm	ε at 273nm (λ_{max1})	ε at 369nm (λ_{max2})
NPWD-3	6801	-	-	14724	-
NPWD-5	5278	616	391	3851	605
NPWD-8	3630	307	212	2743	303

The IR spectra of the pristine silica and the nanopowder-grafted photoinitiators were recorded. The absorption bands corresponding to the photoinitiators are weak, but clearly visible. The broad band at $\nu = 3400$ cm^{-1} in the IR spectrum, corresponding to the silanol groups is very weak for the pristine silica, and does not change, or even gets slightly more intense for the modified nanopowders. This result indicates that there is a polymeric organosilica network attached to the surface of the nanopowder, which is not completely condensed [48]. The presence of photoinitiators was confirmed by the signals corresponding to the carbonyl groups (1750-1600 cm^{-1})

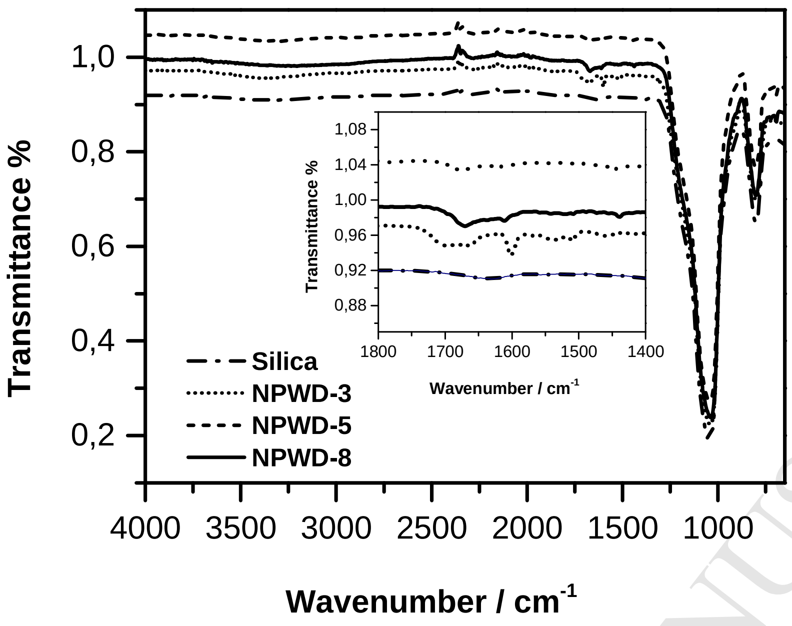

Figure 3. FTIR spectra of the pristine silica and the nanopowder-grafted photoinitiators. The IR bands corresponding to the photoinitiator molecules are magnified in the inset.

Characterization of the reactivity of the nanosilica-grafted photoinitiators

The reactivity of the nanosilica-grafted photoinitiators was evaluated for two different types of polymerization reactions: an acrylate homopolymerization (THFA) and a thiol-ene reaction (HDSH and TATATO)(Scheme 5).

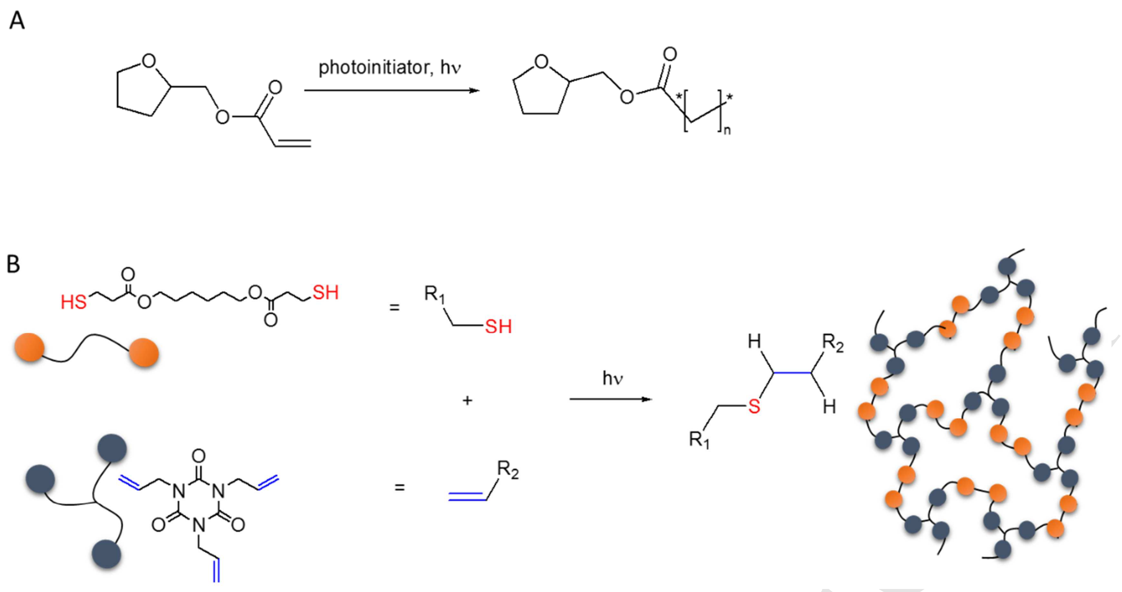

Scheme 5. Systematic representation of thiol-ene and acrylate polymerizations. (A) Polymerization of monofunctional THFA monomer *via* chain growth mechanism. (B) Polymerization of the bifunctional thiol and trifunctional allyl monomer by *via* step growth mechanism.

The radical photopolymerization was monitored by following the decreasing C=C signal at 1620 and 1635 cm^{-1} during irradiation of a thin film. The particle-grafted initiators were compared to their parent phototoinitiators (Fig. 4). Although the performance of all the attached photoinitiators was satisfying, **NPWD-3** and **NPWD-8** showed exceptionally good results, similar to the parent initiators, while **NPWD-5** led to a lower conversion of monomers.

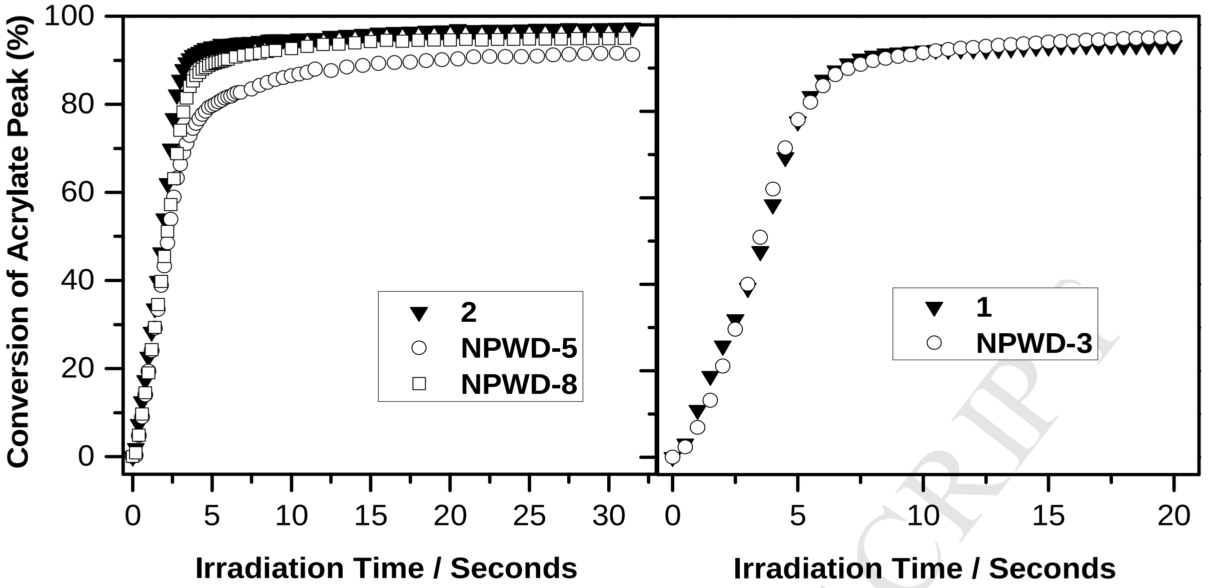

Figure 4. IR kinetics of THFA polymerization for the nanopowder-grafted initiators and their parent initiators **1** and **2**. The depletion of the C=C signal at 1620 and 1635 cm^{-1} was recorded.

The performance of the grafted photoinitiators and their parent compounds in a thiol-ene reaction was studied by monitoring the disappearance of the stretching vibration bands, namely the thiol S-H absorption peak at 2570 cm^{-1} and the allyl C=C absorption peak at 1645 cm^{-1}, during the irradiation of a thin film [23]. For the grafted initiators the final conversion of the allyl and thiol groups was similar or slightly lower than for the non-immobilized initiators, although the rate of the reaction was generally lower for the immobilized initiators (Fig. 5). The best results were obtained for the nanopowder **NPWD-8**. The products **NPWD-5** and **NPWD-3** were significantly slower in initiation than their parent initiators, but the reaction of the thiol and the allyl monomers was proceeding in the correct stoichiometry to reach a high total conversion. Remarkably, when a sample of the nanopowder was used, which had previously been washed multiple times by centrifugation (**NPWD-3-washed**), the polymerization reaction was not affected, proving that any physically attached oligomeric initiators, even if present in small amount, do not play a significant role in the reactivity of the nanopowders.

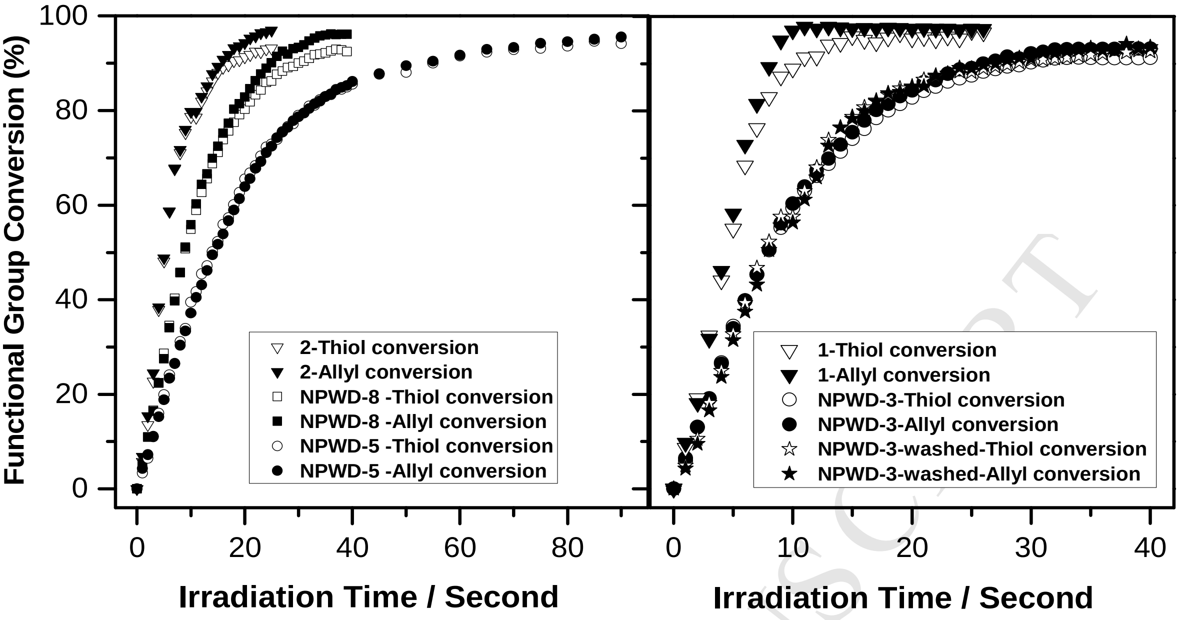

Figure 5. IR kinetics of thiol-ene polymerization for the nanopowder-grafted initiators and their parent initiators **1** and **2**. The depletion of the S-H signal (2570 cm^{-1}) and of the allyl C=C signal at 1645 cm^{-1} was monitored [23].

It is interesting to note that in the thiol-ene reaction, the derivatives of **1** and **2** had comparable efficiency, and the parent photoinitiator **1** even outperformed photoinitiator **2**. Such results are unexpected, since phosphonyl radicals are known to be generally more efficient in initiating polymerization reactions than benzoyl radicals.[50–53] Notably, the expected behaviour was observed in the polymerization of THFA, where the derivatives of **2** performed generally better than the derivatives of **1**.

Structural characterization of a nanocomposite obtained by initiating polymerization from nanopowder-surface

To compare the nanopowder grafted initiator **NPWD-8** to its parent initiator **2**, three different test bodies were prepared, by casting the resin into moulds and photocuring it.

Test body **A**: a nanocomposite of **NPWD-8** in a thiol-ene resin (HDSH/TATATO)

Test body **B**: a nanocomposite of pristine silica nanopowder in a thiol-ene resin (HDSH/TATATO); compound **2** was used as the photoinitiator

Test body **C**: a thiol-ene polymer obtained by the polymerization of HDSH/TATATO, initiated by the non-immobilized initiator **2** (without nanosilica filler).

For these samples, the gel fraction, *i.e.*, the fraction of the sample that is not extractable, was determined using a method previously described [54]. Notably, slightly higher gel fractions were obtained for the nanocomposites, with the nano-powder grafted initiator (test body **A**) hinting at a reaction efficiency as high as the parent initiator (test body **B**) in terms of monomer conversion (inclusion into the network) (Table 6).

Dynamic mechanical thermal analysis (DMA/DMTA) was applied to study the dynamic glass transition region, an indicator of network dynamics of the test bodies. From Table 6, it can be seen that the glass transition occurs at a slightly lower temperature for the composites. Although the difference is not significant, the trend is reproducible and consistent.

The DQ NMR experiments are complementary and more informative than both the techniques mentioned above. The non-network fraction from DQ NMR accounts not only for the free isotropic chains (unreacted monomers or other extractables), that are taken into account in equilibrium swelling experiments (gel fraction), but also for the non-extractable part of the network that are elastically inactive [55]. This 'inelastic network fraction' (non-extractable non-network fraction), obtained from the difference between the gel fraction and the elastic network fraction, can be assumed to consist mainly of non-crosslinked chains (tails) and is thus an excellent indicator of the efficiency of the network formation. Interestingly, the gel fraction of the two composites (test bodies **A** and **B**) is similar and slightly higher than that of the pure polymer material (test body **C**), whereas the elastic network fraction is similar for all measured samples. Thus, the inelastic network fraction shows that crosslinking is more efficient in test body **A** than in test body **B**, though less efficient than in test body **C**.

DQ NMR provides a relative parameter D_{avg} which is inversely proportional to chain mobility, as well as a relative distribution of dynamics ($\sigma/\langle D_{avg}\rangle$)~~,~~ which is a measure of the dynamic heterogeneity in the formed network. The D_{avg} values obtained from DQ NMR agrees with the trend of T_g^{DMA}, indicating that chain motion is fastest in case of test body **A**. Also the distribution or heterogeneity in dynamics is significantly higher for test body **A**. This may result from the large size distribution of the raw **NPWD-8** nanopowder (cf. Fig. 1).

Table 6: Characterization of different UV cured composites **A** – **C** based on thiol-ene resins.

SAMPLE NAME	GEL FRACTION%	T_G^{DMA} (K)	DQ NMR			INELASTIC NETWORK
			(elastic)	D_{avg}	$\sigma/\langle D_{avg}\rangle$	

			Network fraction (%)	[kHz]		FRACTION (%)*
TEST BODY A	97.07 ±1.61	261.4	95.1 ±0.97	6.40	0.73	2.0
TEST BODY B	97.14 ±1.08	261.9	94.4 ±0.86	6.92	0.66	2.7
TEST BODY C	95.99 ±1.04	262.2	95.2 ± 0.94	7.09	0.66	0.8

* Obtained from the difference between gel and network fractions.

To demonstrate the applicability of the particle-grafted photoinitiator **NPWD-8** in photolithography, we tested the patterned polymerization of tris[2-(acryloyloxy)ethyl] isocyanurate, and thiol-ene resins through a photomask. After irradiation, the unpolymerized (*i.e.*, soluble) resin was washed off. The resulting structures were compared to those obtained with the parent photoinitiator **2** (Fig. 6). Photolithographic patterning was proven possible, which confirms that the particles are homogenously dispersed in the resin. However, it can be noticed that the edges and the surface of the patterned structures are rougher when the nanopowder-grafted initiators are used.

Figure 6. Curing experiments with the use of a photomask (25 µm). (A) Photoinitiator **2**, and (B) **NPWD-8** in the acrylate based resin. (C) Photoinitiator **2**, and (D) **NPWD-8** in the thiol-ene resin.

III. Conclusion and Outlook

We synthesized and characterized six different trialkoxysilyl-functionalized photoinitiators, some of which are reported for the first time. The silanes generally exhibit very good photoreactivity, comparable or even improved when compared to their parent photoinitiators. Especially the new silane-functionalized photoinitiator **8**, derived from initiator **2** and APTES, shows excellent reactivity and can be obtained in good yield. We believe that it may find future applications in material science.

Three selected silane-functionalized photoinitiators (**3**, **5** and **8**) have been successfully immobilized on the surface of fumed silica. To obtain a higher level of surface modification, a practical method was developed for the surface immobilization. Most of the initiator molecules (>90%) were proven to be covalently grafted to the silica surface.

The fumed silica nanopowder, although commonly used, is a mediocre carrier for surface grafted photoinitiators. This is because of its aggregated structure and broad size distribution of the grains. Also, importantly, the low silanol content on the surface of fumed silica nanopowders makes it a difficult target for silanization. Regarding the low silanol content at the surface, most of the photoinitiators are expected to form a highly crosslinked polymeric shell around the particles. The influence of the polymeric, rather than monolayer structure of the nanoparticle shell is currently under investigation.

Nonetheless, it was proven that particle grafted photoinitiators successfully polymerize acrylic monomers and thiol-ene resins. The polymerization of acrylic resins was very efficient and the nanopowder grafted initiators performed similarly to the free (*i.e.*, non-immobilized) parent photoinitiators.

In thiol-ene polymerization, in which diffusion plays a major role, the grafted initiators performed slightly slower than the free initiators.

It was found that chain dynamics in composites of **NPWD-8** was slightly faster than in silica filled and unfilled networks obtained with the parent initiator, although its dynamic heterogeneity was more pronounced. Interestingly, the inelastic network fraction consisting primarily of chain ends was significantly lower for composites of **NPWD-8**, compared with the composite of pristine silica, indicating that the efficiency of crosslinking was better with the surface grafted initiators.

It was demonstrated that the macroscopic distribution of the nanopowder in the resin is sufficient to be used in patterned polymerization with a photomask.

A detailed study of the mobility of the nanopowder-grafted photoinitiators and their extractables is currently underway and will be reported in a forthcoming contribution.

IV. Experimental

Materials

Dichloromethane, 2-butanone, triethylamine, 3-(triethoxysilyl)propyl isocyanate, sodium iodide, (3-glycidyloxypropyl)trimethoxysilane, oxalyl chloride, (3-aminopropyl)triethoxysilane (APTES), (3-mercaptopropyl)trimethoxysilane (MPTMS), trifluoroacetic acid, 1,3,5-triallyl-1,3,5-triazine-2,4,6(1H,3H,5H)-trione (TATATO), tris[2-(acryloyloxy)ethyl] isocyanurate and silica nanopowder with a specific surface area (BET) of 175-225 m^2/g were supplied by Sigma-Aldrich. Tetrahydrofurfuryl acrylate (THFA) and 2-hydroxy-4′-(2-hydroxyethoxy)-2-methylpropiophenone (1) were provided by TCI. Silica gel (Normasil 60) 40-63 µm, technical grade toluene, ethyl acetate and ethanol (96%) were purchased from VWR. (3-glycidyloxypropyl)triethoxysilane was purchased from ABCR. Ethyl 2,4,6-trimethylbenzoylphenylphosphinate (2) was provided by courtesy of BASF. All chemicals were used as received. 1,6-hexane bis(3-mercaptopropionate) (HD-SH) was synthesized according to previous literature. [56,57]

NMR

^{1}H-NMR and ^{13}C-NMR spectra were recorded on a Varian 400-NMR spectrometer operating at 399.66 and 100.5 MHz, respectively, and were referenced to $Si(CH_3)_4$. For the acquisition of the ^{1}H-NMR spectra a relaxation delay of 10 s and a 458 pulse were used. The NMR spectra were referenced to solvent residual peaks according to values given in the literature [58]. Reprints of the NMR spectra are presented in the Supporting Information.

LRMS

MS spectra were recorded on a Quatro LC Micromass and LCT Micromass TOF apparatus. Reprints of the NMR spectra and the MS spectrograms are presented in the Supporting Information.

1-{4-[2-(3-triethoxysilanylpropylcarbamoyloxy)ethoxy]-phenyl}-2-hydroxy-2-methyl-1-propane-1-one (3)

To a suspension of **1** (10.0 g, 44.6 mmol) in toluene (100 mL) stirred at 70 ˚C triethylamine (622 µL, 4.46 mmol) and 3-(triethoxysilyl)propyl isocyanate (13.25 mL, 53.5 mmol) were added and the resulting suspension was stirred at this temperature for 24 h. After stirring for 2 h, a clear solution was obtained. The solution was concentrated under reduced pressure and the residual oil was purified by column chromatography on silica gel using CH_2Cl_2-AcOEt (gradient 0-50% AcOEt) as eluent. The purified product was a pale yellow oil, which solidified quickly to form a white residue (18.0 g, 38.2 mmol, 86%).

^{1}H NMR (400 MHz, $CDCl_3$): δ = 0.62 (t, J = 8 Hz, 2H), 1.21 (t, J = 8 Hz, 9H), 1.58-1.62 (m, 8H), 3.16-3.21 (m, 2H), 3.78-3.83 (q, J = 8 Hz, 6H), 4.18-4.25 (m, 2H), 4.38-4.36 (m, 2H), 5.05 (bs, 1H-NH), 6.95 (d, J = 8 Hz, 2H), 8.05 (d, J = 8 Hz, 2H), ppm.

^{13}C NMR (100 MHz, $CDCl_3$): δ = 7.6, 18.3, 23.2, 28.7, 43.4, 58.4, 62.6, 66.7, 75.8, 114.1, 126.1, 132.4, 156.1, 162.4, 202.6, ppm.

LRMS (ESI): [M + Na]+ 494.1.

Sodium 2,4,6-trimethylbenzoylphenylphosphinate [33]

To a solution of **2** (15.00 g, 47.4 mmol) in 2-butanone (80 mL) stirred at room temperature, anhydrous NaI (7.819 g, 52.2 mmol) was added. After 10 min, a pale orange solution was obtained. This solution was heated in an oil bath to 60 ˚C and stirred at this temperature for 24 h. The product started precipitating after approximately 10 min. The suspension was cooled to room temperature and was filtered under reduced pressure, washed with cold 2-butanone (2x50 mL) and diethylether (2x40 mL) and dried on air. A white solid (10.6 g, 34.2 mmol, 72%) was obtained, which was directly used in the next step.

2,4,6-Trimethylbenzoylphenylphosphinic acid (4) [33]

A solution of sodium 2,4,6-trimethylbenzoylphenylphosphinate (9.40 g, 30.2 mmol) in distilled water (60 mL) was vigorously stirred at room temperature. Dilute aqueous H_2SO_4 (0.5 M, 33 mL) was added to reach a pH≈1. The product precipitated gradually during addition. To the resulting suspension ethyl acetate (300 mL) was added and after vigorous mixing the phases were separated. The aqueous layer was additionally extracted with ethyl acetate (2x100 mL). The combined organic layers were washed with distilled water (2x50 mL) and dried over anhydrous Na_2SO_4. After evaporation of the solvent under reduced pressure 8.40 g (29.1 mmol, 96%) of a pale yellow solid was obtained.

^{1}H NMR (400 MHz, CDCl$_3$): δ = 1.99 (s, 6H), 2.22 (s, 6H), 6.71 (s, 2H), 7.37-7.42 (m, 2H), 7.52-7.57 (m, 1H), 7.67-7.72 (m, 2H), 10.81 (s, 1H-OH), ppm.

^{13}C NMR (100 MHz, CDCl$_3$): δ =19.3, 21.2, 127.0, 128.4 (d, 3J = 13 Hz), 128.4, 132.5 (d, 2J = 10 Hz), 133.0 (d, 4J = 3 Hz), 134.4, 136.2 (d, 1J = 47 Hz), 139.6, 215.6 (d, J = 117 Hz), ppm.

1,1-dimethoxy-3-[methyl(2,4,6-trimethylbenzoyl)phenylphosphininate]-2,5-dioxa-1-silacyclooctane (5) and (2,4,6-trimethylbenzoyl)phenylphosphinic acid -2-hydroxy-[3-(3-trimethoxysilyl)propyloxy] propyl ester (5-L)

A solution of **4** (5.0 g, 17.3 mmol) in anhydrous toluene (70 mL) was stirred at 60 ˚C for 10-15 min to obtain a clear solution. A solution of (3-glycidyloxypropyl)trimethoxysilane (3.83 mL, 17.3 mmol) in toluene (10 mL) was added and the resulting solution was stirred at 60 ˚C for 6 h. After cooling to room temperature the solution was washed with 2% (w/w) aqueous Na_2CO_3 solution (3x25 mL), 1% aqueous citric acid solution (2x25 mL), distilled water (25 mL) and was dried over anhydrous Na_2SO_4. After evaporation of the solvent, the residual oil was purified by column chromatography on silica gel using CH_2Cl_2-AcOEt (gradient 0-50% AcOEt) as the eluent. The purification gave 3.0 g (6.1 mmol, 35%) of product in the form of a colorless oil.

^{1}H NMR (400 MHz, CDCl$_3$): δ = 0.67-0.73 (m, 2H), 1.66-1.76 (m, 2H), 2.14 (s, 2H), 2.16 (s, 4H), 2.26 (s, 3H), 3.15-3.23 (m, 1H), 3.35-3.40 (m, 1H), 3.48 (s, 3H), 3.52-3.53 (m, 3H), 3.61-3.66 (m, 1H), 3.72-3.77 (m, 1H), 4.02-4.09 (m, 2H), 4.17-4.25 (m, 1H), 6.81-6.82 (m, 2H), 7.46-7.51 (m, 2H), 7.59-7.63 (m, 1H), 7.80-7.87 (m, 2H), ppm.

^{13}C NMR (100 MHz, CDCl$_3$): δ = 7.1, 7.1*, 19.4*, 19.4, 21.1, 23.7, 50.4* (d, J = 20 Hz), 50.5 (d, J = 26 Hz), 65.7 (d, J = 8 Hz), 65.8* (d, J = 8 Hz), 71.4 (d, J = 6 Hz), 71.5* (d, J = 6 Hz), 72.0, 72.1*, 72.6, 72.7*, 125.5 (d, J = 123 Hz), 125.6* (d, J = 123 Hz), 128.6, 128.6*, 128.8, 128.8*, 132.9* (d, 3J = 10 Hz), 133.0 (d, 3J = 10 Hz), 133.4, 133.5*, 134.4, 134.4*, 136.4* (d, 1J = 47 Hz), 136.5 (d, 1J = 47 Hz), 140.0, 140.0*, 214.8* (d, J = 113 Hz), 214.8 (d, J = 113 Hz), ppm.

LRMS (ESI): [M + Na]+ 515.0.

As the second fraction, 485 mg (5%) of the product **5-L**, containing minor impurities, was obtained as an oil.

^{1}H NMR (400 MHz, CDCl$_3$): δ = 0.61-0.65 (m, 2H), 1.62-1.69 (m, 2H), 2.13 (s, 6H), 2.26 (s, 3H), 3.31-3.41 (m, 3H), 3.55 (s, 9H), 3.64-3.82 (m, 2H), 3.93-3.98 (m, 1H), 4.06-4.22 (m, 2H), 6.81 (s, 2H), 7.47-7.52 (m, 2H), 7.60-7.63 (m, 1H), 7.81-7.86 (m, 2H), ppm.

1,1-diethoxy-3-(methyl (2,4,6-trimethylbenzoyl)phenylphosphininate) -2,5-dioxa-1-silacyclooctane (6) and (2,4,6-trimethylbenzoyl)phenylphosphinic acid 2-hydroxy-(3-(3-trimethoxysilyl)propyloxy) propyl ester (6-L)

A solution of **4** (500 mg, 1.73 mmol) in anhydrous toluene (70 mL) was stirred at 60 ˚C for 10-15 min to obtain a clear solution. A solution of (3-glycidyloxypropyl)triethoxysilane (0.450 mL, 1.73 mmol) in toluene (10 mL) was added and the resulting solution was stirred at 60 ˚C for 6 h. After cooling to room temperature the solution was washed with 2% (w/w) aqueous Na_2CO_3 solution (3x25 mL), 1% aqueous citric acid solution (2x25 mL), distilled water (25 mL) and was dried over anhydrous Na_2SO_4. After evaporation of the solvent, the residual oil was purified by column chromatography on silica gel using CH_2Cl_2-AcOEt (gradient 0-50% AcOEt) as the eluent. The purification gave 155 mg (0.3 mmol, 17%) of product in the form of a colorless oil.

^{1}H NMR (300 MHz, $CDCl_3$): δ = 0.68-0.75 (m, 2H), 1.16-1.22 (m, 6H), 1.68-1.78 (m, 2H), 2.15 (d, J = 0.3 Hz, 3H), 2.17 (d, J = 0.3 Hz, 3H), 2.27 (s, 3H), 3.15-3.23 (m, 1H), 3.36-3.45 (m, 1H), 3.60-3.67 (m, 1H), 3.71-3.84 (m, 6H), 4.00-4.08 (m, 2H), 4.18-4.29 (m, 1H), 6.82-6.83 (m, 2H), 7.49-7.52 (m, 2H), 7.59-7.64 (m, 1H), 7.81-7.88 (m, 2H), ppm.

^{13}C NMR (75 MHz, $CDCl_3$): δ = 8.3, 8.3*, 18.5, 19.6, 21.4, 24.2, 58.4* (d, J = 2.3 Hz), 58.6, 66.0* (d, J = 3.7 Hz), 66.1 (d, J = 3.7 Hz), 71.5 (d, J = 6.7 Hz), 71.7* (d, J = 6.7 Hz), 72.4, 72.5*, 73.0, 73.0*, 126.7 (d, J = 123 Hz), 126.8* (d, J = 123 Hz), 128.8*, 128.8, 129.0, 129.0*, 133.1* (d, 3J = 8.2 Hz), 133.2 (d, 3J = 8.2 Hz), 133.6, 1336*, 134.6, 134.6*, 136.6* (d, 1J = 46.5 Hz), 136.7 (d, 1J = 47.2 Hz), 140.2*, 140.2, 215.1* (d, J = 113 Hz), 215.1 (d, J = 113 Hz), ppm.

LRMS (ESI): [M + Na]+ 543.0.

As the second fraction, 51 mg (0,098 mmol, 6%) of the product **6-L** was obtained as an oil.

^{1}H NMR (400 MHz, $CDCl_3$): δ = 0.58-0.62 (m, 2H), 1.18-1.22 (m, 9H), 1.61-1.68 (m, 2H), 2.13 (s, 6H), 2.26 (s, 3H), 3.35-3.43 (m, 4H), 3.77-3.82 (m, 6H), 3.91-3.99 (m, 1H), 4.05-4.23 (m, 2H), 6.79-6.81 (m, 2H), 7.46-7.51 (m, 2H), 7.59-7.62 (m, 1H), 7.80-7.87 (m, 2H), ppm.

2,4,6-Trimethylbenzoylphenylphosphinic acid chloride (7)

To a suspension of **4** (5.00 g, 17.3 mmol) in dichloromethane (40 mL), which was stirred at room temperature, oxalyl chloride (2.93 mL, 34.6 mmol) was added in small portions. The evolution of gas bubbles was observed. The mixture was stirred at room temperature for 20 h, during which it gradually became a clear solution. After evaporation under reduced pressure, dry toluene (50 mL) was added to the residual oil, and was evaporated again to dryness at 50 ˚C to give a pale brown oil (5.30 g, 17.2 mmol, quant.) which was used in next step without further purification.

(2,4,6-trimethylbenzoyl)phenylphosphinic acid *N*-(3-(triethoxysilyl)propyl) amide (8)

To a solution of (3-aminopropyl)triethoxysilane (8.10 mL, 34.6 mmol) in anhydrous toluene (50 mL), which was stirred at room temperature, the solution of **7** (5.30 g, 17.2 mmol) in anhydrous toluene (20 mL) was added and the resulting mixture was stirred for 1 h. The reaction mixture was washed with distilled water (30 mL), 1% (w/w) aqueous citric acid solution (3x25 mL) then with 2% (w/w) aqueous Na_2CO_3 solution (2x25 mL), again with distilled water (25 mL) and was then dried over anhydrous Na_2SO_4. After evaporation of the solvent, the residual oil was purified by column chromatography on silica gel, using CH_2Cl_2-AcOEt (gradient 0-20% AcOEt) as the eluent. The purification gave product **8** in the form of a colourless oil (6.35 g, 12.9 mmol, 75%).

^{1}H NMR (400 MHz, $CDCl_3$): δ = 0.60-0.64 (m, 2H), 1.20 (t, J = 8 Hz, 9H), 1.65-1.69 (m, 2H), 2.03 (s, 6H), 2.22 (s, 3H), 2.97-3.01 (m, 2H), 3.79 (q, J = 8 Hz, 6H), 6.74 (s, 2H), 7.41-7.44 (m, 2H), 7.51-7.53 (m, 1H), 7.75-7.80 (m, 2H), ppm.

^{13}C NMR (75 MHz, $CDCl_3$): δ = 7.7, 18.5, 19.6, 21.3, 25.7 (d, J = 6 Hz), 42.8 (d, J = 2.3 Hz), 58.6, 127.9, 128.7 (d, 3J = 12.8 Hz), 132.9 (d, 4J = 3 Hz), 133.5 (d, 2J = 9 Hz), 134.5, 136.5 (d, 1J = 43.5 Hz), 140.0, 215.1 (d, J = 100.5 Hz), ppm.

LRMS (ESI): [M + Na]+ 514.3, [2M + Na]+ 1005.6.

(2,4,6-trimethylbenzoyl)phenylthiophosphinic acid *S*-(3-(trimethoxysilyl)propyl) ester (9)

To a mixture of (3-mercaptopropyl)trimethoxysilane (3.25 mL, 17.5 mmol), triethylamine (4.80 mL, 34.5 mmol) and anhydrous toluene (50 mL), which was stirred at room temperature, the solution of **7** (5.30 g, 17.2 mmol) in toluene (20 mL) was added and the resulting suspension was stirred at this temperature for 1 h. The reaction mixture was washed with distilled water (30 mL), 1% (w/w) aqueous citric acid solution (3x25 mL) then with 2% aqueous Na_2CO_3 solution (2x25 mL), again with distilled water (25 mL) and was then dried over anhydrous Na_2SO_4. After evaporation of the solvent, the residual oil was purified by column chromatography on silica gel, using CH_2Cl_2-AcOEt (gradient 0-

20% AcOEt) as the eluent. The purification gave product **9** in the form of a colourless oil (4.09 g, 8.8 mmol, 51%).

^{1}H NMR (400 MHz, $CDCl_3$): δ = 0.65-0.69 (m, 2H), 1.70-1.74 (m, 2H), 2.12 (s, 6H), 2.26 (s, 3H), 2.83-2.89 (m, 2H), 3.50 (s, 9H), 6.81 (s, 2H), 7.47-7.50 (m, 2H), 7.55-7.57 (m, 1H), 7.87-7.91 (m, 2H), ppm.

^{13}C NMR (75 MHz, $CDCl_3$): δ = 8.8, 19.9, 21.4, 21.2, 24.6 (d, J = 4.5 Hz), 31.5 (d, J = 3 Hz), 50.5, 128.4, 128.9 (d, 3J = 30.8 Hz), 132.4 (d, 2J = 9.8 Hz), 133.1 (d, 4J = 3 Hz), 135.0, 135.6 (d, 1J = 47.3 Hz), 140.7, 214.6 (d, J = 73.5 Hz), ppm. HRMS (ESI): m/z calcd. for $C_7H_9Br_2N_2$ [M + H]+ 343.8108, found 343.8105.

_N_-(3-(trimethoxysilyl)propyl)-2,4,6-trimethylbenzamide (10)

A solution of **8** (100 mg, 0.200 mmol) in anhydrous toluene (2.0 mL) was stirred at 80 ˚C. To this solution (3-aminopropyl)triethoxysilane (45 mg, 0.20 mmol) was added and the mixture was stirred for 24 h. The progress of the reaction was controlled by TLC (20% AcOEt in DCM). After cooling to room temperature, the reaction mixture was washed with distilled water (2x2.0 mL) and dried over anhydrous Na_2SO_4. After removal of the solvent, the residual oil was purified by column chromatography on silica gel using CH_2Cl_2-AcOEt (gradient 0-10% AcOEt) as the eluent. The purification gave 45 mg (0,122 mmol, 61%) product **10** as a colourless solid.

^{1}H NMR (300 MHz, $CDCl_3$): δ = 0.66-0.72 (m, 2H), 1.19 (t, J = 6 Hz, 9H), 1.68-1.78 (m, 2H), 2.26 (s, 3H), 2.28 (s, 6H), 3.41-3.48 (m, 2H), 3.80 (q, J = 6 Hz, 6H), 5.98 (t, J = 6 Hz, 1H), 6.82 (m, 2H), ppm.

^{13}C NMR (75 MHz, $CDCl_3$): δ = 8.2, 18.4, 19.3, 21.2, 23.1, 42.1, 58.6, 128.3, 134.2, 135.4, 138.4, 170.6, ppm.

LRMS (ESI): [M + Na]+ 390.2, [2M + Na]+ 757.6.

Immobilization of the photoinitiators on the surface of silica nanopowder *via* silanization

General method 1

Product **3** was grafted to the silica nanopowder, as previously reported. [23] First, the silica particles were exposed to a corona dosage of 833 W min m^{-2}. Then, 5.0 g corona treated particles were dispersed in 180 mL of anhydrous dichloromethane by sonication. Silane **3** (250 mg; 5% w/w of silica particles) were separately dissolved in 20 mL of anhydrous dichloromethane and added to the reaction mixture, which was then heated to reflux temperature (55 ˚C) and stirred for additional 3 h.

Then the reaction mixture was divided into several centrifugation tubes and centrifuged for 100 min at 4000 rpm. The supernatant was discarded and the particles were dried at 60 °C for overnight. To remove the physically attached polycondensate, the powder was dispersed in acetone by sonication and then centrifuged at 4000 rpm for 100 min. The washing was repeated 3 times and the particles were dried overnight at 60 ˚C.

General method 2

A suspension of silica nanopowder (24.0 g) in toluene (550 mL) was stirred at room temperature. A solution of silane (7.2 mmol) in toluene (50 mL) was added and the resulting suspension was vigorously stirred for 24 h. After this time trifluoroacetic acid (1.0 mL) and ethanol (96%, 50 mL) were added and the reaction mixture was stirred for further 24 h, after which it was evaporated to dryness on a rotary evaporator (bath temperature set to 50 ˚C). The dry residue was re-suspended in ethanol (96%, 400 mL) by sonication for 20 min to obtain a homogenous suspension. Trifluoroacetic acid (1.0 mL) was added and the mixture was stirred at room temperature overnight. The solvent was evaporated and the hydrolysis/condensation in EtOH was repeated. After evaporation of the solvent, the residue was suspended in toluene (200 mL) by sonication, and the solvent was removed on a rotary evaporator. Additional drying under high vacuum (0.1 mbar) at room temperature over 48 h gave the product in the form of a white, slightly aggregated powder. A fine powder could be obtained by gentle grinding of the solid residue in a mortar.

(NPWD-3) Modification of silica nanopowder with 3

Product **3** (3.40 g, 7.2 mmol) was used for the silanization and 26.1 g of **NPWD-3** was obtained, which had an initiator concentration of 0.273 mmol/g.

(NPWD-5) Modification of silica nanopowder with 5 (1/2 scale)

Product **5** (1.77 g, 3.6 mmol) was used for the silanization and 13.71 g of **NPWD-5** was obtained, which had an initiator concentration of 0.266 mmol/g.

(NPWD-8) Modification of silica nanopowder with 8 (1/2 scale)

Product **8** (1.77 g, 3.6 mmol) was used for the silanization and 13.53 g of **NPWD-8** was obtained, which had an initiator concentration of 0.271 mmol/g.

Photo-DSC

The photo-DSC experiments were performed on a NETZSCH photo-DSC 204 F1 Phoenix. All measurements were conducted at 50 °C in aluminum crucibles under nitrogen atmosphere. The sample quantity was 8.00 (± 0.05) mg of resin [1 wt% or 5 wt% of the photoinitiator in THFA]. The Omnicure s2000 was used as the light source at 1 W/cm^2 resulting in an intensity of 80 mW/cm^2 at the surface of the sample (range of wavelength was 250 – 445 nm). For the determination of the reaction enthalpy and t_{max}, the samples were illuminated twice for 10 min each with an idle time of 2 min in between. For the analysis, the second run was subtracted from the first one to obtain the reaction enthalpy curve.

Transmission electron microscopy (TEM)

To investigate the differently treated silica nanopowders, they were dissolved in methanol and drop casted on carbon grids. To avoid agglomeration, the solutions were sonicated for 1 min prior to drop casting. TEM was carried out using a Phillips CM12, operated at 120 kV. Bright-field TEM images at different magnifications were acquired to analyze the size distribution and morphology of the nanoparticles.

IR

FT-IR spectroscopy was carried out with a Vertex 70 spectrometer (Bruker, US). Typically 16 scans were taken with 4 cm^{-1} resolution, in the range of 4000-800 cm^{-1}.

For the characterization of the nanopowders, approx. 15 mg of the dry product was pressed using a hydraulic press (Perkin Elmer). The obtained pellets were subjected to FTIR measurements using the ATR mode.

Crosslink kinetics were characterized by real-time Fourier Transform Infrared Spectroscopy (FTIR) measurements. Resin mixtures were formulated by mixing equal molar ratio of thiol groups of HD-SH monomer with C=C double bond groups of TATATO for the thiol-ene reaction. As a monofunctional acrylate monomer THFA was used. For the commercial initiators (**1** or **2**) 1% (w/w) of the initiator was added directly to the resin mixture. In the case of the nanopowder-bound initiators, the amount of nanopowder was adjusted to fit the total molar concentration of 1% (w/w) **1** and 1% (w/w) **2**, respectively. A dispersion of the nanoparticles in chloroform was used to facilitate homogenization The resin formulations were spin-casted on CaF$_2$ discs, and after evaporation of the chloroform, the thin films were irradiated with an Omnicure S1000 high pressure Hg lamp (λ=250-470 nm; Lumen Dynamics; Canada) under nitrogen atmosphere for the thiol-ene system. For the acrylate system, the thin film was placed between two CaF_2 plates. The power density P was set to 1.35 mW cm^{-2} for the thiol-ene system and to 25 mW cm^{-2} for the acrylate system. The intensity of the light in the sample plane was measured with an integrating radiometer (Powerpuck II, EIT Instrument Markets, US). The reaction kinetics were followed by FTIR, until maximum conversion was reached. The conversions of the thiol, allyl and acrylate functional groups were calculated using OPUS 7.0 Spectrum software.

Functional group conversion was calculated based on equation (1),where $\boldsymbol{A_0}$ and $\boldsymbol{A_t}$ are normalized peak areas of the characteristic IR stretching vibrations prior to and after a selected time of UV exposure.

$$\%\ \textbf{Func. Group Conversion} = \left[\frac{\boldsymbol{A_0 - A_t}}{\boldsymbol{A_0}}\right] * \mathbf{100} \tag{1}$$

UV-Vis spectroscopy

UV-Vis measurements were carried out with a Varian (United States) Cary 50 UV-Vis spectrophotometer in absorbance mode. For sample preparation, certain amounts of samples were dispersed in 10 mL acetonitrile by sonication. UV-Vis spectra of samples were taken in a quartz cell with 0.1 cm path length.

TGA

Thermogravimetric analysis was conducted with a Perkin Elmer Pyris 7 under oxygen atmosphere. The samples were heated from 25 to 900°C with a heating rate of 4 K/min and kept at 900 °C for 30 min.

Elemental analysis

Determination of C, H, N and S was done on a Eurovector EA 3000 CHNS-O Elemental Analyser. Digestion/mineralisation of the sample material was achieved by “flash combustion®“, applying 25 kPa oxygen at 1000 ˚C. Determination of P was performed by colorimetric determination as "molybdene blue" [59].

MALDI TOF

The samples were washed by centrifugation in acetone and redispersion *via* sonication (3 cycles, 15 min, 3500 g). The collected supernatants were evaporated to dryness, and contained a significant amount of small silica nanoparticles (approx. 90%). Samples **NPWD-3**, **NPWD-5** and **NPWD-8** were wetted with a minimal amount of CH_2Cl_2 and placed on the target (2-3 mg; MTP 384 target plate, ground steel BC, Bruker Daltonics). Samples **Ext-NPWD-3**, **Ext-NPWD-5** and **Ext-NPWD-8** were first redispersed in a minimal amount of chloroform and then filtered through a 0.2 µm PTFE syringe filter to separate most of the silica nanopowder. The residues were then evaporated, redispersed in CH_2Cl_2 (100 mg/mL) and placed on the target (1 µL). For all samples, a volume of 1 µL of the matrix solution [30 mg/mL 2,5-dihydroxybenzoic acid in 0.1% (v/v) aqueous TFA : acetonitrile (4 : 6)] was added on the target and allowed to crystallize. The measurement was performed on an autoflex speed MALDI-TOF instrument (Bruker Daltonics) in the positive-ion/reflectron mode with individually optimized laser pulse energy in the range of m/z 530-5600.

Preparation of the test bodies A, B and C

Three different resin mixtures were formulated for comparison of mechanical properties. All resins were prepared by mixing an equimolar thiol bond concentration of HD-SH with an equimolar C=C double bond concentration from TATATO. Then, 0.5 (w/w) of **2** (total matrix weight was considered in all calculations) as an initiator was added to form resin A. Resin B was prepared by addition of 11.7% (w/w) of **NPWD-8** to the thiol-ene mixture. Here, the molar amount of attached initiator on **NPWD-8** matches the molar amount of **2** in the first mixture. Resin C was prepared by adding 0.5 (w/w) of **2** and 10.5% (w/w) of pristine silica particles to the thiol-ene mixture.

The resins were poured into home-made rectangular-shaped PDMS moulds with a thickness of 0.5 mm. Photo-curing of the free-standing films was conducted under nitrogen atmosphere using an Hg lamp (Light hammer 6 UV curing system, Fusion UV Systems, United States, with a wavelength range between 250 and 470 nm). The exposure dose in the sample plane was 213.52 mJ/cm² (measured with an external radiometer) per irradiation cycle. Twelve irradiation cycles were applied for each sample.

Dynamic mechanical thermal analysis (DMA/DMTA)

DMA measurements were carried out in tensile mode on specimen cast of preformed moulds of dimensions 20 mm x 4 mm (Perkin Elmer DMA800). The sample thickness was measured individually at 5 different regions of the sample and an average value was taken. After clamping the sample (clamping length = 10 mm), it was cooled to 213 K at a rate of 5 K/min using liquid N_2. Then the measurements were carried out at a frequency of 1 Hz at a heating rate of 3 K/min until about 313 K (+60 ˚C) at 0.125% strain (12.5 µm strain amplitude), after applying a static pre-force of 0.3 N; corresponding to a static displacement of about 10 µm. The glass transition temperature was determined from the zero-crossing of the first derivative of tan δ.

Swelling measurements

Gel contents of cured samples were calculated through swelling measurements. Rectangular samples with a mass of 50 ±10 mg were cut and submerged into chloroform (20 mL). After 24 h the samples were taken out and dried with a tissue. After 48 h of drying at 50 ˚C, gel fractions were calculated from dried weights, according to equation (2).

$$\%\,\mathbf{Gel\ Content}\ =\left[\frac{\boldsymbol{m_{dry}}}{\boldsymbol{m_0}}\right]*\mathbf{100} \qquad (2)$$

Low field NMR

NMR measurements were carried out on a Bruker Minispec mq20 desktop low field NMR spectrometer operating at a ^{1}H-NMR frequency of 19.5 MHz and a permanent magnet with a field strength of 0.47 T. The 90°/180° pulses were optimized for each sample and the values ranged between 2.6-2.7 μs and 5.1-5.2 μs respectively. The dwell time was kept short in order to have a spectral width of at least 1.25 MHz and the signal was acquired up to 0.5 ms. The samples were punched in the form of disc and stacked in a 8 mm tube up to a height of 5 mm and placed in the middle of the homogeneous part of the magnetic field for measurements. The samples were then heated with dry air. A BVT3000 temperature controller was used for temperature regulation. The measurements were carried out at 100 ±0.1 ˚C after equilibrating the samples at this temperature for about 20 min.

For the recording of DQ build-up curves as a function of excitation (and reconversion) times, $\tau_{exc/rec}$, Baum-pines pulse sequence [60] in a slightly modified form [61] as well as the 3-pulse (also known as 5-pulse) DQ sequence [62] was used. The integral of the real part of the complex in-phase on-resonance signal for each excitation time was used to get the intensity of each point. This intensity data was subjected to normalization as per the now common procedure which helps determining the non-elastic fraction as well as producing a dynamics-free multiple-quantum build-up curve. Complete details of the experiment and the procedure for normalization can be found in several manuscripts [61], [55], [63], [64]. After the above mentioned normalization procedure, in order to get a distribution curve (average D_{avg} and the distribution σ of the dipolar couplings), the normalized double quantum curves (nDQ) were inverse Laplace-transformed using a numerical inversion procedure based on Gaussian function as kernel and fast Tikhonov regularization. [see eq 4 in [65]]

Preparation of negative toned photoresists

Thin resin films were drop-casted on glass microscope slides and irradiation was performed through a 25 µm-patterned quartz mask in non-contact mode using a high pressure Hg lamp (Omnicure S1000, Lumen Dynamics, Canada) with an exposure dose of 162 mJ/cm^2. Development of negative tone photoresists were done by dipping the microscope slides in acetone for a few seconds. Patterns were displayed using an optical microscope (Olympus/Japan & BX51 Color View IIIu Soft Imaging System/ Germany).

Acknowledgements:

This research was conducted within the lead-project AddManu.at, funded by the Austrian Research Promotion Agency (Forschungs-Förderungsgesellschaft FFG). Part of this study was performed at the Polymer Competence Center Leoben GmbH (PCCL, Austria) within the framework of the Comet K1 program and the “Produktion der Zukunft” program of the Austrian Federal Ministry for Transport, Innovation and Technology and of the Austrian Federal Ministry for Economy, Family and Youth with contributions of University of Leoben. PCCL is funded by the Austrian Government and the State Governments of Styria, Lower Austria and Upper Austria.

PR and MS contributed equally to this work. We thank Dr. Martin Zehl from the Center for Mass Spectroscopy, University of Vienna for valuable discussions regarding the MALDI-TOF results and Mag. Johannes Theiner from the Microanalytical Laboratory, University of Vienna for performing the Elemental analysis. We also thank Johanna Klobasa for help during the FTIR-kinetics measurements.

References

[1] Fouassier JP, Rabek JF. Radiation curing in polymer science and technology. London, New York: Elsevier Applied Science, 1993.

[2] Allen NS (ed.). Photochemistry and photophysics of polymer materials: Wiley, 2010.

[3] Lee J, Shim G, Park J, Kim H, Han K. Int. J. Adhes. Adhes. 2016;70:249–59.

[4] Mostegel FH, Roth M, Gassner M, Oesterreicher A, Piock R, Edler M et al. Prog. Org. Coat. 2016;94:116–23.

[5] Fouassier JP, Burr D, Crivello JV. J. of Macromolecular Sc., Part A 1994;31(6):677–701.

[6] Stampfl J, Baudis S, Heller C, Liska R, Neumeister A, Kling R et al. J. Micromech. Microeng. 2008;18(12):125014.

[7] Griesser T, Wolfberger A, Daschiel U, Schmidt V, Fian A, Jerrar A et al. Polym. Chem. 2013;4(5):1708.

[8] Pawar AA, Saada G, Cooperstein I, Larush L, Jackman JA, Tabaei SR et al. Science Advances 2016;2(4).

[9] Heller C, Pucher N, Seidl B, Kalinyaprak-Icten K, Ullrich G, Kuna L et al. Journal of Polymer Science Part A: Polymer Chemistry 2007;45(15):3280–91.

[10] Li Z, Siklos M, Pucher N, Cicha K, Ajami A, Husinsky W et al. Journal of Polymer Science Part A: Polymer Chemistry 2011;49(17):3688–99.

[11] Allen NS, Marin MC, Edge M, Davies DW, Garrett J, Jones F et al. Journal of Photochemistry and Photobiology A: Chemistry 1999;126(1-3):135–49.

[12] Hu L, Shi W. Chinese Journal of Chemistry 2011;29(9):1961–8.

[13] Hu L, Shi W. Composites Part A: Applied Science and Manufacturing 2011;42(6):631–8.

[14] Sangermano M, Periolatto M, Castellino M, Wang J, Dietliker K, Grützmacher JL et al. ACS Appl. Mater. Interfaces 2016;8(30):19764–71.

[15] Dietliker K, Hüsler R, Birbaum J, Ilg S, Villeneuve S, Studer K et al. Prog. Org. Coat. 2007;58(2-3):146–57.

[16] Advincula RC. Journal of Dispersion Science and Technology 2003;24(3-4):343–61.

[17] Kamigaito M, Ando T, Sawamoto M. Chem. Rev. 2001;101(12):3689–746.

[18] Barbey R, Lavanant L, Paripovic D, Schüwer N, Sugnaux C, Tugulu S et al. Chemical Reviews 2009;109(11):5437–527.

[19] Werne T von, Patten TE. Journal of the American Chemical Society 2001;123(31):7497–505.

[20] Ohno K, Koh K, Tsujii Y, Fukuda T. Macromolecules 2002;35(24):8989–93.

[21] Hui CM, Pietrasik J, Schmitt M, Mahoney C, Choi J, Bockstaller MR et al. Chemistry of Materials 2014;26(1):745–62.

[22] Sangermano M, Periolatto M, Castellino M, Wang J, Dietliker K, Grützmacher JL et al. ACS Applied Materials & Interfaces 2016;8(30):19764–71.

[23] Sahin M, Schlögl S, Kaiser S, Kern W, Wang J, Grützmacher H. Journal of Polymer Science Part A: Polymer Chemistry 2016:n/a-n/a.

[24] Huber A, Kuschel A, Ott T, Santiso-Quinones G, Stein D, Bräuer J et al. Angewandte Chemie International Edition 2012;51(19):4648–52.

[25] Wang J, Siqueira G, Muller G, Rentsch D, Huch A, Tingaut P et al. Chem. Commun. 2016;52(13):2823–6.

[26] Arai H. Inorganic particle dispersions, cured films thereof, and their manufacture(JP5471522).

[27] Arai H. Preparation of inorganic particle dispersions forming hard coatings with excellent scratch resistance.(JP2011157435).

[28] Choi H, Cho CH. Method of manufacturing flexible display device using UV-decomposable silane compound to easily detach flexible display board from carrier board(KR 2014136560).

[29] GUANGZHOU BOSSIN POLYMERIZATION MATERIALS CO. LTD. 一种含硅氧烷基团的长波吸收光引发剂及其制备方法 Containing siloxane groups of the long-wave absorption of light initiator and its preparation method: Google Patents, 2015; Available from: http://google.com/patents/CN103333276B?cl=en.

[30] Muhr N, Puchleitner R, Kern W. European Polymer Journal 2013;49(10):3114–24.

[31] Peled A, Naddaka M, Lellouche J. J. Mater. Chem. 2011;21(31):11511–7.

[32] Mendonca CR, Correa DS, Baldacchini T, Tayalia P, Mazur E. Applied Physics A 2008;90(4):633–6.

[33] Noe R, Henne A, Maase M. Acyl- and bisacylphosphine derivatives: Google Patents, 2009; Available from: https://www.google.com/patents/US7511084.

[34] Oesterreicher A, Roth M, Hennen D, Mostegel FH, Edler M, Kappaun S et al. European Polymer Journal 2017;88:393–402.

[35] Honma T, Kubota T, Kiyomori A. Aqueous solution of piperazinyl-containing silanol compound and making method(JP 5499963).

[36] Honma T. Chromium-free surface treatment agent and method for surface treatment of metal therewith(JP 2012111983).

[37] Honma T, Kubota T, Kiyomori A. Organosilicon compound and process for the preparation thereof(JP 5359584).

[38] Honma T, Kubota T, Tonomura Y. Amino-containing organosilicon compound and making method: Google Patents, 2017; Available from: http://www.google.com/patents/US20170002030.

[39] Bade S, Seliger B, Schladerbeck N, Sauer J. Process for preparing glycidyloxyalkyltrialkoxysilanes: Google Patents, 2011; Available from: https://encrypted.google.com/patents/US8039646.

[40] Honma T, Kubota T, Kiyomori A. Organosilicon compound having amino group and its production method: Google Patents, 2011; Available from: https://www.google.ch/patents/US8049027.

[41] Honma T. Adhesive compositions containing organosilicon compound having piperazinyl groups and fillers and metals treated with them(JP 5699462).

[42] Kreutzkamp N, Schindler H. Archiv der Pharmazie 1960;293(3):296–305.

[43] Segall Y, Shirin E, Granoth I. Phosphorus and Sulfur and the Related Elements 1980;8(2):243–54.

[44] Harger, Martin J. P., Westlake S. Tetrahedron 1982;38(10):1511–5.

[45] Hoz S, Dunn EJ, Buncel E, Bannard, R. A. B., Purdon JG. Phosphorus and Sulfur and the Related Elements 1985;24(3):321–6.

[46] Wyatt P, Eley H, Charmant J, Daniel BJ, Kantacha A. European Journal of Organic Chemistry 2003;2003(21):4216–26.

[47] Abell JP, Yamamoto H. Journal of the American Chemical Society 2009;131(42):15118–9.

[48] Gallas J, Goupil J, Vimont A, Lavalley J, Gil B, Gilson J et al. Langmuir 2009;25(10):5825–34.

[49] Jiang SP. Materials Science and Engineering: A 2006;418(1):199–210.

[50] Salmassi A, Eichler J, Herz, C.P., Schnabel, W., W. Schnabel. Polymer Photochemistry 1982;2(3):209–18.

[51] Kuhlmann R, Schnabel W. Die Angewandte Makromolekulare Chemie 1978;70(1):145–57.

[52] Kuhlmann R, Schnabel W. Polymer 1977;18(11):1163–8.

[53] Kuhlmann R, Schnabel W. Polymer 1976;17(5):419–22.

[54] Sahin M, Ayalur-Karunakaran S, Manhart J, Wolfahrt M, Kern W, Schlögl S. Advanced Engineering Materials 2017;19(4):1600620-n/a.

[55] Saalwächter K. Progress in Nuclear Magnetic Resonance Spectroscopy 2007;51(1):1–35.

[56] Wutticharoenwong K, Soucek MD. Macromolecular Materials and Engineering 2008;293(1):45–56.

[57] Wutticharoenwong K, Soucek MD. Journal of Applied Polymer Science 2009;113(4):2173–85.

[58] Gottlieb HE, Kotlyar V, Nudelman A. The Journal of Organic Chemistry 1997;62(21):7512–5.

[59] Taylor AE, Miller CW, Roth H. Mikrochemie 31:292, 1944.

[60] Baum J, Pines A. Journal of the American Chemical Society 1986;108(24):7447–54.

[61] Saalwächter K, Ziegler P, Spyckerelle O, Haidar B, Vidal A, Sommer J. The Journal of Chemical Physics 2003;119(6):3468–82.

[62] Voda MA, Demco DE, Perlo J, Orza R, Blümich B. Journal of Magnetic Resonance 2005;172(1):98–109.

[63] Valentín JL, Posadas P, Fernández-Torres A, Malmierca MA, González L, Chassé W et al. Macromolecules 2010;43(9):4210–22.

[64] Malmierca MA, González-Jiménez A, Mora-Barrantes I, Posadas P, Rodríguez A, Ibarra L et al. Macromolecules 2014;47(16):5655–67.

[65] Haba D, Barbezat M, Ayalur-Karunakaran S, Schlögl S, Brunner AJ, Pinter G. Journal of Polymer Science Part B: Polymer Physics 2016;54(17):1738–47.

Highlights

New silane-functionalized photoinitiators show excellent reactivity.

Particle grafted photoinitiators polymerize acrylic monomers and thiol-ene resins.

The grafted initiators perform similarly to the free photoinitiators.